Composite Structures 92 (2010) 1913–1919

Contents lists available at ScienceDirect

Composite Structures

journal homepage: www.elsevier.com/locate/compstruct

A smart multifunctional polymer nanocomposites layer for the estimation of low-velocity impact damage in composite structures

F. Capezzuto [a], F. Ciampa [b], G. Carotenuto [a], M. Meo [b,*], Eva Milella [c], F. Nicolais [d]

[a] Institute of Composite and Biomedical Materials (IMCB-CNR), National Research Council, Piazzale Tecchio, 80 – 80125 Napoli, Italy
[b] Material Research Centre, Department of Mechanical Engineering, University of Bath, Bath, UK
[c] IMAST s.c.ar.l. – Technology Cluster, P.le E. Fermi, 1 – 80055 Portici (Napoli), Italy
[d] Dipartimento di Scienza della Comunicazione, Università di Salerno, Via Ponte don Melillo, I-84084, Fisciano, Salerno

ARTICLE INFO

Article history:
Available online 20 January 2010

Keywords:
Nanocomposites
Smart layer
Low-velocity impact
Fluorescence

ABSTRACT

A new smart polymer nanocomposite layer, based on semiconductor Cu_2S nanoparticles embedded into an amorphous polystyrene matrix, was developed for the detection of low-velocity impact damage on composite structures. This material exhibits a combination of optical and electro-magnetic properties, in way that it can be employed to visualize in quick and effective manner barely visible impact damage (BVID). In particular, based on the phenomenon of the photoluminescence, this layer showed specific light emission in the visible range of the electromagnetic spectrum under UV-light excitation at different wavelength. The results of a series of low-velocity impact tests illustrated a visible contrast colour on the damaged area, representing the flaw. In fact, the study of the optical characteristics of this smart material is of particular benefit for fast, cost-effective and *in situ* damage identification. Hence, once the impact location has been determined, the detailed information of the damage can be further investigated by others non-destructive techniques.

1. Introduction

With the growing interest to use laminar composite materials in aircraft structures, much attention is devoted to the development of rapid, accurate and cost-effective *built-in* systems for the detection and evaluation of the defects. Damages due to low-velocity impact events not only weaken the structure undergone to a continuous service load, but also may generate different types of flaws before full perforation, i.e. sub-surface delamination, matrix cracks, fibre debonding or fracture, indentation and barely visible impact damage (BVID). Over time, these effects can induce variations in the mechanical properties of such composites structures (the primary effect of a delamination is to change the local value of the bending stiffness and of the transverse-shear stiffness), leading to possible catastrophic failure conditions.

For this reason, a number of different non-destructive evaluation techniques (NDT) and Structural Health Monitoring (SHM) systems used for aircraft inspection, including acoustic emission (AE), X-ray, thermography, shearography and ultrasonic inspection, can efficiently detect the impact location source and characterize existing and emerging defects. These detection methods are classified in two different approaches known as *active* and *passive techniques*. The first approach is based on searching the defect generated by a probe directly on the specimen surface, while in the *passive technique*, the signals emitted by external or internal sources are measured [1]. However both approaches often rely on complex and expensive systems, difficulties in interpreting results etc.

A possible solution for the low-velocity impact detection might be found by using a smart layer with ad hoc developed properties (optical, magnetic etc.) to be embedded or attached to a structure to be monitored.

One possible solution can be obtained by developing a smart layer with tailored optical properties where semiconductor Cu_2S nanoparticles embedded into a matrix through a simple and effective *in situ* chemical approach.

These smart materials are perfectly transparent and colourless and are able to show light at different wavelength by simply changing the excitation frequency (Fig. 1) [2–10]. In addition, nanoscopic semiconductors embedded into optical plastics (PS, PMMA, PC, etc.) may exhibit a combination of electric and magnetic properties not available in any of the individual constituents [10–13]. This characteristic of "*multi-functionality*" makes this material potentially employable in a wide range of technological applications for SHM, as it could provide quick information on damage location.

The objective of the research work illustrated in this paper was to report the results of the development and characterisation of the optical behaviour of a new smart polymer nanocomposites layer to be use as a low-velocity impact passive detection.

* Corresponding author.
E-mail address: M.Meo@bath.ac.uk (M. Meo).

0263-8223/$ - see front matter © 2010 Elsevier Ltd. All rights reserved.
doi:10.1016/j.compstruct.2010.01.003

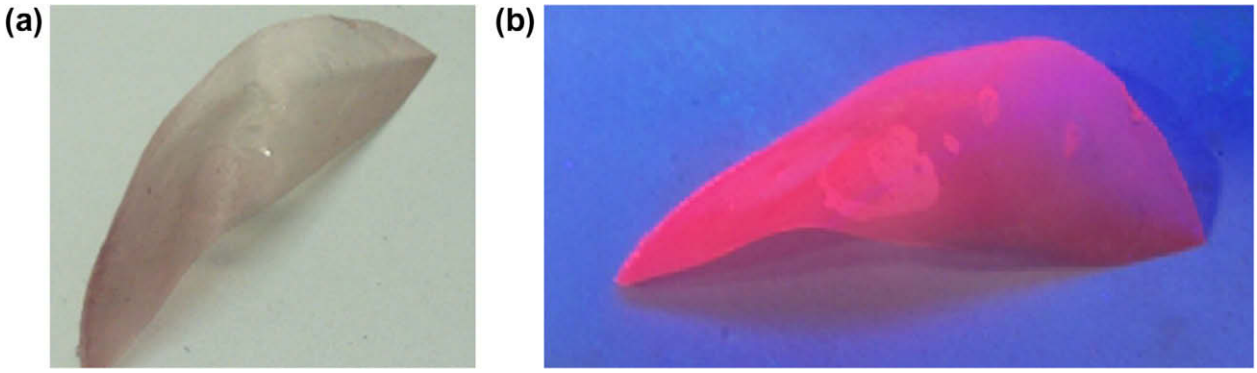

Fig. 1. Fluorescent nanocomposite film observed under visible light (a) and under ultraviolet light at the wavelength of 365 nm (b).

This smart layer could be employed in a triple-use mode: layered (1) on the impacted face and (2) smart on the backface (3) combination of modes 1 and 2. The mode 1 inspection would be mainly for both monolithic composite and sandwich structures. Scratches, dents, or strikes would cause the layer to break or change the concentration of the nanoparticles and therefore visual inspections for colour disruption or colour intensity changes of the paint would easily allow inspectors to pinpoint potentially damaged areas.

In the case of mode 2 it is mainly for monolithic structures. Under low-velocity impacts while the surface may appear to be undamaged upon visual inspection, hidden delaminations may appear beneath the impacted surface. Such damage is called barely visible impact damage (BVID). In addition, internal damages lead to significant reduction in local strengths and can slowly grow under alternating or fluctuating stress leading to a loss in stiffness and ultimately to catastrophic failures. It is therefore important to be able to image back-surface damage and monitor damages in high loaded composite components to receive an early warning for a well timed maintenance of the aircraft.

To estimate impact damage on the back-face in accessible area the use of a probe radiating light at the excitation frequency would be sufficient. In inaccessible areas, the use of small robots or *in situ* permanently installed devices would allow the aircraft maintenance operators to detect BVID.

This smart layer would provide a quick and efficient way to identify the impact location, then the characteristics of the impact damage might be further investigated by more accurate non-destructive techniques.

In this work, the layer developed was widespread on the surface of a variety of laminated plates, subsequently damaged with low-velocity impacts, and then radiated with ultraviolet light of different wavelength (300–400 nm) to check how colour intensity changes or disruption could be used to highlight cracked areas. In particular, the presence of defects as matrix cracks, fibre bridging and delamination was observed by a fluorescence emission extending in the visible spectral region, from 600 up to 800 nm [2,6,9]. This phenomenon is related to the increase of the band-gap energy value, because of the conduction and valence band contraction due to the lower number of atoms present in a nanoscopic phase compared to the bulk [4,7].

The layout of the paper is as follows: the second Section describes the synthesis, the morphological-structural characterization by Transmission Electron Microscopy (TEM) and X-ray Powder Diffraction (XRD), and the study of the optical and fluorescence characteristics of Cu_2S nanoparticles embedded in amorphous polystyrene. Section 3 provides the results on the previous analysis whilst in Section 4 the experimental procedure for impact damage evaluation in different laminated composite plates is illustrated. Then, the conclusions of the paper are reported.

2. Experimental methodology

Copper(I) sulfide, Cu_2S, is a semiconductor with interesting fluorescence characteristics that to the best of our knowledge has never been described in the literature. Nanoparticles of Cu_2S dispersed into an optical polystyrene matrix were produced by a chemical technique based on the *in situ* decomposition of a mercaptide precursor (i.e., copper(I) dodecyl-mercaptide, $CuSC_{12}H_{25}$) dissolved in polymer [4,5].

The copper(I) dodecyl-mercaptide, $CuSC_{12}H_{25}$, was prepared by adding drop-by-drop an alcoholic solution of dodecanethiol, $C_{12}H_{25}SH$ (Aldrich), to a copper(II) chloride solution, $CuCl_2$ (Aldrich, 99.9%) in ethanol (99.8%) at room-temperature, under stirring. Stoichiometric amounts of reactants were used. The mercaptide promptly precipitated as a white crystalline powder, which was separated by vacuum-filtration and then washed several times with ethanol. According to the literature [14], this reaction involved two steps: in the first step, the cupric ion was reduced to cuprous ion by thiol; in the second step, the obtained cuprous ion and thiol combine together to generate the mercaptide compound, which is not soluble in ethanol:

$$2Cu^{2+} + 2C_{12}H_{25}SH \rightarrow 2Cu^{+} + (SC_{12}H_{25})_2 + 2H^{+} \quad (1)$$

$$Cu^{+} + C_{12}H_{25}SH \rightarrow 2Cu^{+} + CuSC_{12}H_{25} + H^{+} \quad (2)$$

In order to prepare mercaptide/polymer blends, a little amount of copper(I) dodecyl-mercaptide was dissolved in chloroform and mixed with a chloroform solution of amorphous polystyrene (M = 230,000 $gmol^{-1}$, Aldrich). The obtained system was accurately homogenized with ultrasounds, then cast onto a glass-substrate and dried in air at room temperature. The dried films of Cu(I) dodecyl-mercaptide/polystyrene blend were opalescent and white, these films were converted to the Cu_2S/polystyrene nanocomposite by thermal annealing at ca. 200 °C for 15 s. During the heat treatment, the films became quite transparent and yellow–brown coloured, because of the mercaptide crystals melting and molecular dissolution into the polymer. The mercaptide thermal decomposition led to the formation of copper(I) sulfide nanoparticles, according to the following chemical reaction [14]:

$$2CuSC_{12}H_{25} \rightarrow Cu_2S + S(C_{12}H_{25})_2 \quad (3)$$

The thermolysis of pure copper(I) dodecyl-mercaptide was studied by Thermogravimetric Analysis (TGA, TA INSTRUMENTS 2950) and Differential Scanning Calorimetry (DSC, TA INSTRUMENTS 2920). The Cu_2S nanoparticles morphology produced by

in situ $CuSC_{12}H_{25}$ thermal decomposition were obtained analyzing nanocomposite films by Transmission Electron Microscopy (TEM, Philips EM208S microscope equipped with a MegaView Room for digital images acquisition, at acceleration voltage of 100 kV). The crystalline nature of nanoparticles embedded in polymer was investigated by X-ray Diffraction (XRD, Rigaku DMAX-IIIC). The optical characteristics of nanocomposite films were obtained by absorption and emission optical spectroscopy, using a UV–Vis Spectrophotometer (Perkin-Elmer Lambda-850) and a Fluorescence Spectrometer (Perkin-Elmer-LS55), respectively.

3. Experimental analysis and results

The Thermogravimetric Analysis (TGA) was carried out by heating the pure copper(I) dodecyl-mercaptide sample from room temperature to 800 °C, at 10 °C/min, under fluxing nitrogen. This TGA showed the formation of copper(I) sulfide at a temperature of ca. 200 °C (the residual weight percentage exactly corresponded to the Cu_2S percentage in the mercaptide). The Differential Scanning Calorimetry (DSC) runs were performed from 50 °C to 350 °C, at 10 °C/min rate, under fluxing nitrogen and using sealed aluminium caps (Fig. 2). The DSC thermogram showed several endothermal signals that corresponded to:

(i) the liquid–crystalline transition (lamellar–columnar) at a temperature of 104 °C (onset-point),
(ii) the columnar-phase melting at a temperature of ca. 142 °C (onset-point),
(iii) the mercaptide thermal decomposition at ca. 206 °C (onset-point),
(iv) broad endothermic peak in the range 190–260 °C, probably corresponding to the evaporation of decomposition by-product (i.e., docecyl-thioetere, $S(C_{12}H_{25})_2$) [7] (Fig. 2b).

The nanocomposite film inner morphology was obtained by Transmission Electron Microscopy (TEM). The micrograph given in Fig. 3 shows a contact-free dispersion of spherically shaped copper(I) sulfide nanoparticles. The nanoparticles had a monomodal, symmetric (Gaussian), and quite tight particle size distribution characterized by an average diameter of ca. 6.8 nm with a standard deviation of 1.1 nm (TEM micrographs were analyzed using the SigmaScan-Pro5 image analysis program).

The nature of the solid phase generated in the polymeric matrix by copper(I) mercaptide thermal decomposition was established by X-ray Powder Diffraction (XRD) analysis of the nanocomposite films. XRD was performed using CuKα radiation (λ = 0.154056 nm).

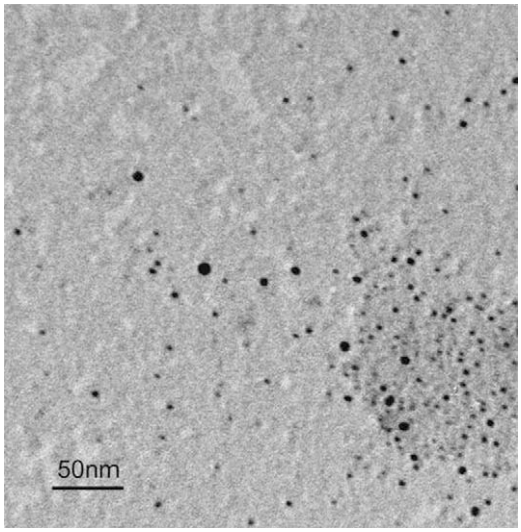

Fig. 3. TEM-micrograph of Cu_2S nanoparticles embedded in polystyrene matrix.

The detection range was 2θ = 5–80°, with step and scanning rate of 0.02° and 8 s/step, respectively. The nanoscopic inorganic phase was isolated from the polymer by dissolution/centrifugation, and XRD was carried out on the pure powder (Fig. 4).

As visible, the diffraction pattern is exactly corresponding to that of a monoclin Cu_2S standard [16]. The main peaks are those of the following crystalline planes: (2 3 1), (3 3 1), (4 1 3), (7 2 1), (1 0 6) and (7 0 6). The obtained results agree with the JCPDS 33-490 file. An approximate estimation of the nanoparticles size was achieved by applying the Scherrer's equation to the strong (2 3 1) signal, and an average size value of 10 nm resulted. Such crystallite size resulted larger than the average size obtained by TEM investigation (i.e., ca. 6.8 nm) because of the XRD implicit overestimation due to the absence of diffraction contribution coming from the smallest crystals.

The optical properties of Cu_2S/polystyrene films were obtained by absorption and emission spectroscopy. The film UV–Vis spectrum is shown in Fig. 5.

As visible, the spectrum seems to contain two peaks: one strong at a wavelength of 357 nm and another broad and of low intensity at 420 nm. The last peak caused the nanocomposite film yellow colouration.

The precursor $CuSC_{12}H_{25}$/polystyrene blend was not fluorescent, while the Cu_2S/polystyrene nanocomposite film obtained

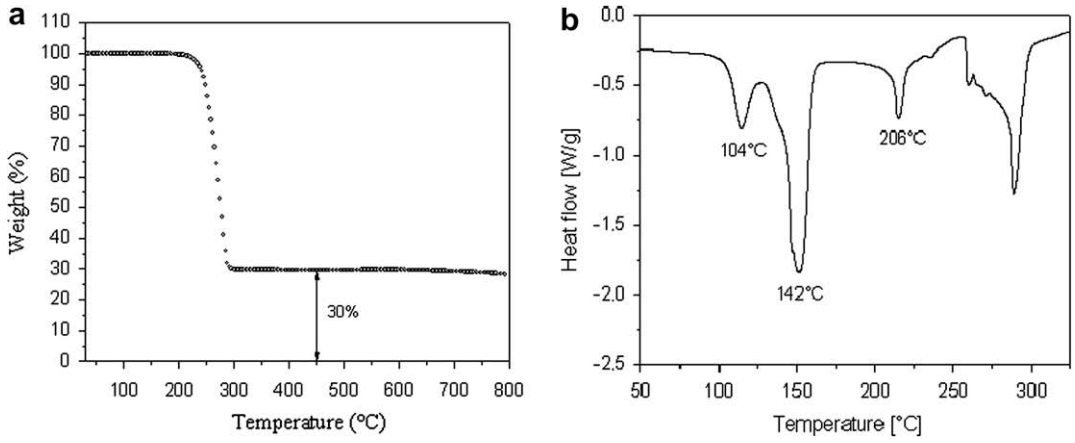

Fig. 2. TGA (a) and DSC (b) thermograms of pure copper(I) dodecyl-mercaptide.

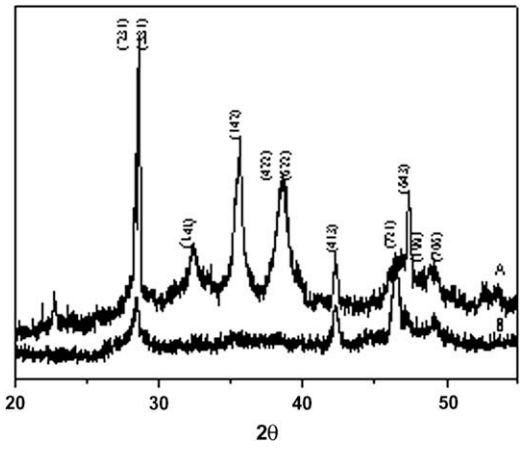

Fig. 4. XRD-diffractogram of Cu_2S/polystyrene nanocomposite film.

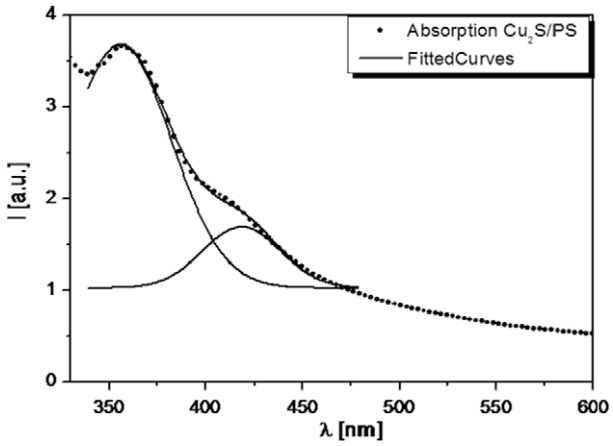

Fig. 5. UV–V is spectrum of the Cu_2S/polystyrene nanocomposite film.

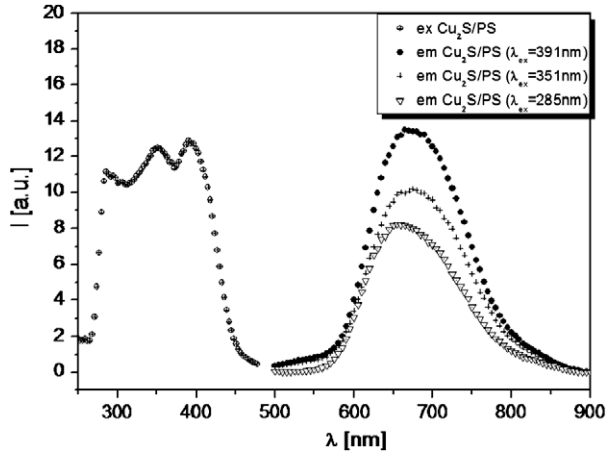

Fig. 6. Excitation and emission spectra of the Cu_2S/polystyrene nanocomposite film.

after thermal annealing resulted quite fluorescent and able to emit an orange–red light by exposure to an UV–lamp (λ_{exc} = 365 nm, 8 W). The fluorescence characteristics of the nanocomposite film were accurately studied by fluorimetry. The excitation and emission spectra are given in Fig. 6, whilst the deconvoluted emission

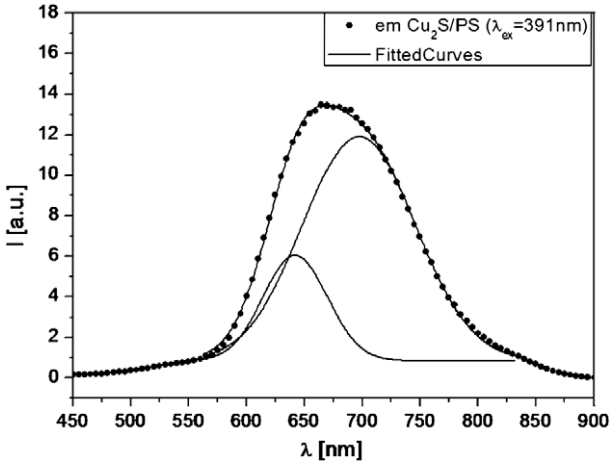

Fig. 7. Deconvoluted emission spectrum of Cu_2S/polystyrene nanocomposite film.

spectrum at the excitation wavelength of 391 nm is depicted in Fig. 7.

The excitation spectrum of Cu_2S nanoparticles embedded in polystyrene was characterized by the presence of a large band uniformly extending over the 280–430 nm spectral range. In particular, three maxima of similar intensities were visible at 286 nm, at 351 nm, and 391 nm. The emission characteristics of film were studied at each one of these three maximum excitation values. It is noted that exciting the sample with these three lightly different wavelengths, the emission peak position did not change but only differences of intensity were observed. The maximum intensity was obtained by exciting the film at 391 nm. In particular, the emission peak, produced by excitation at 391 nm, can be convoluted in two signals: the first consisted of a very intensive and tight symmetric emission band with maximum at 642 nm, the other contained a broad band of low intensity with a maximum at 697 nm (Fig. 7). According to the peak shape and positions, the first emission band should correspond to the semiconductor nanoparticle band-edge emission, whilst the second emission band can be attributed to a band-trap emission (i.e., a fluorescence emission generated by defects present on the surface of Cu_2S nanoparticles). The band-gap energy of the copper(I) sulfide was estimated by the wavelength value of the maximum emission peak convoluted which corresponded to the band-edge emission, according to the following relationship: $E_g = hc/\lambda_{em}$. The Cu_2S band-gap energy value was found to be ca. 1.93 eV, which resulted of 0.73 eV higher than the value of the bulk-semiconductor, which is 1.2 eV [17]. Such effect is related to quantum confinement characterizing the semiconductor phases on a nanometric scale. The observed emission phenomenon is a result of a change in the density of electronic energy levels. In the nanoscale regime, the band-gap of semiconductor materials is size dependent, allowing size-tunable optical properties [7,10]. Finally, it should be observed that the fluorescence characteristics of the produced nanocomposite films were not stable over the time. In fact, after a few months from preparation the material presented a quenching phenomenon, probably caused by the cuprous-sulfide disproportion to zero-valent copper and cupric-sulfide (i.e., $Cu_2S \rightarrow Cu + CuS$) [15].

4. Evaluation of impact damage

The study of the optical properties of the developed composite systems by means of spectrofluorimetric and spectrophotometric analysis showed specific light emission in the visible range under UV-light excitation and absence of plasmon absorption (colourless character) [4,5]. These properties, induced by nanophase quantum

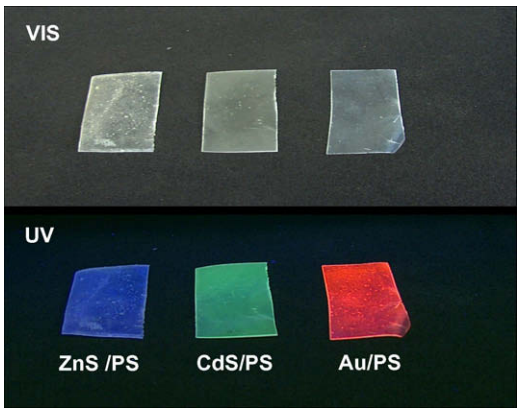

Fig. 8. Polymeric nanocomposites, based on ZnS, CdS and Au nanoparticles into amorphous polystyrene, under Visible and UV (λ_{exc} = 365 nm) radiation exposure.

size effects, can be finely tuned for specific applications tailoring the nanoparticles composition and size through annealing time and temperature, as well as through the polymer type (which influences the nanoparticles size and shape). The nanocomposites with *Au*, *CdS* and *ZnS* quantum dots (i.e. small nanoparticles with the mean size <2 nm) exhibit photoluminescent phenomena which generate red, green and blue light emission under UV-radiation, respectively (Fig. 8).

Hence, in order to evaluate the behaviour of the polymer nanocomposites layer under low-velocity impacts, several experiments were carried out. Initially, this layer was spread on the front/back face of two different composite structures: a carbon fibre reinforced plastic (CFRP) and a sandwich composite plate. Subsequently, different impact loads with energy ranging from 7 to 10 J were applied in order to introduce a BVID damage. Then, the specimen's surface was radiated with ultraviolet light at different wavelength (300–400 nm). Fig. 9 illustrates the experimental procedure.

4.1. Evaluation impact damage on CFRP panel

In the first experiment the polymer nanocomposite material was spread on both front/back surfaces of a AS4/8552 composite plate with dimensions 40 cm × 12 cm × 3 mm with lay-up sequence of $[90/45/45/90]_{3s}$.

The impact with energy of approximately 7 J was applied in the upper part of the specimen using a hand-held modal hammer to generate a BVID. During the test, the panel was clamped along using four edges. To detect the damage, both surfaces were illuminated with UV light at the wavelength of 350 nm (Figs. 10 and 11).

In particular, Fig. 10 illustrates the capability of the smart layer to be used in mode 1. Under BVID conditions, a small dent is present on the impacted face that is difficult to detect. The results show that the smart nanocomposite layer is clearly damaged and a clearly visible contrast colour of the damaged region was produced, representing the flaw when illuminated with UV light.

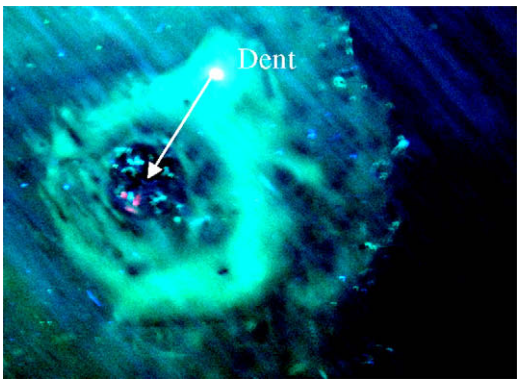

Fig. 10. Front surface of carbon fibre composite plate under UV radiation exposure.

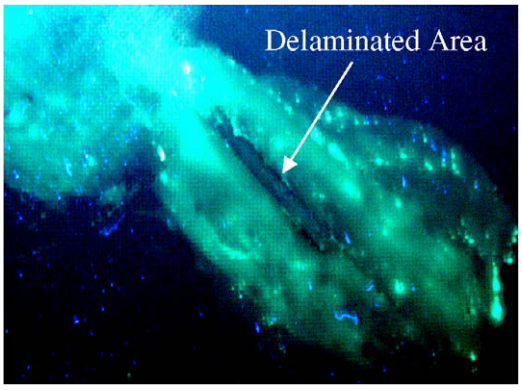

Fig. 11. Back surface of carbon fibre composite plate under UV radiation exposure.

In Fig. 11, the impacted backface is shown. For thin walled structures, back-face delamination and fibre breakage is a common form of damage. The results shows clearly that the smart layer is clearly capable of showing that damage has occurred in a quick, easy and reliable manner and that can be used in mode 2.

These results show that even if the layer spread was not uniform, the presence of the damage can be well recognized using a probe able to emit UV light.

4.2. Evaluation impact location on sandwich panel

The smart nanocomposite layer was also investigated on composite sandwich panels. This type of structures exhibit different failure modes than monolithic composite structures. Under low-velocity impact, honeycomb exhibit local indentation, transverse core crushing, skin delamination and skin/core debonding. For this, the smart material was spread only on the front surface (mode 1). A sandwich composite panel with dimension of (Fig. 12a–d) 0.4 m long and 0.30 m wide. The core used in the sandwich panel was a

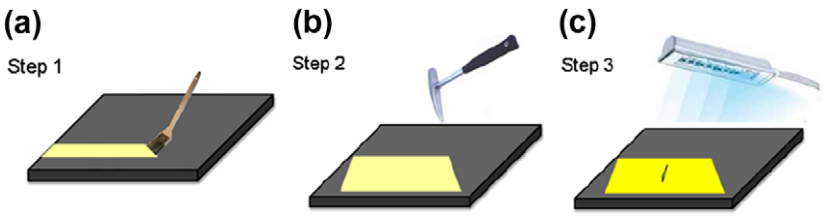

Fig. 9. Experimental procedure. (a) Smart layer was spread on the front/back surface of two different composite structures (CFRP and sandwich panel). (b) Specimens were impacted. (c) Specimens were illuminated with ultraviolet light.

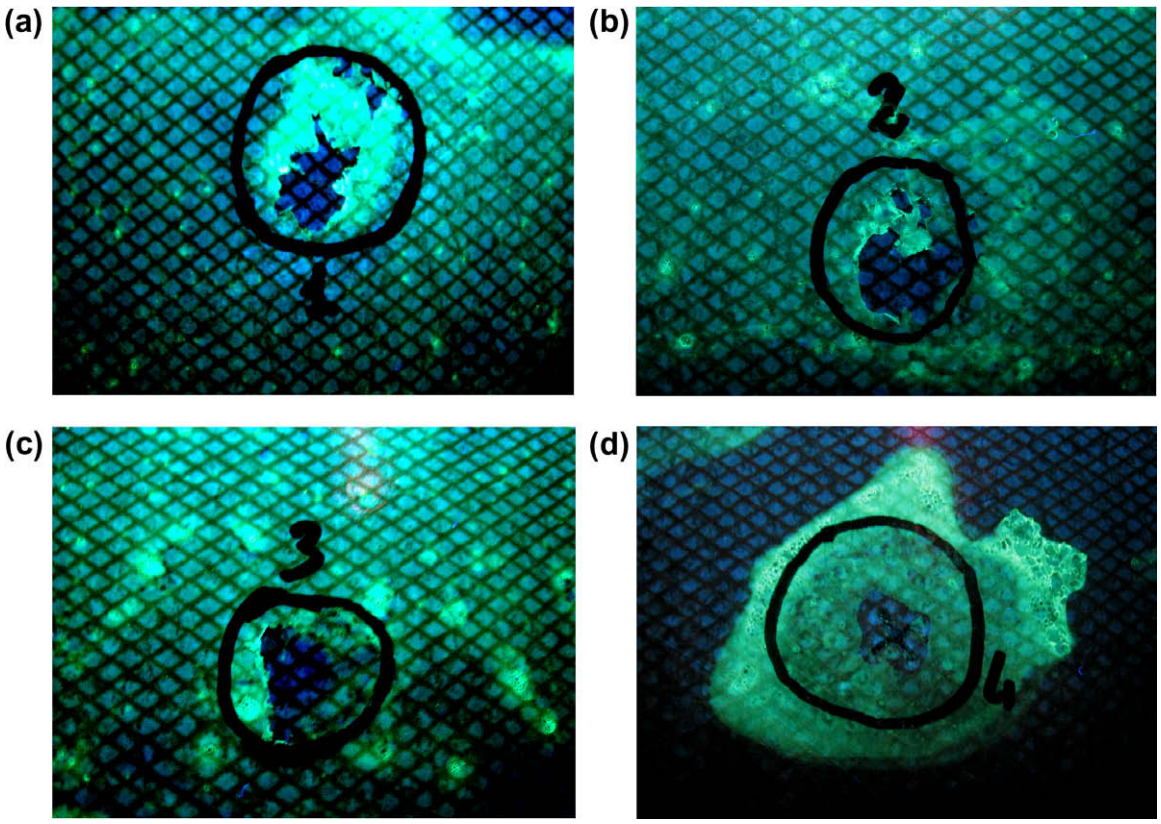

Fig. 12. (a)–(d) Impact on front surface of carbon fibre composite plate under UV radiation exposure.

0.00635 m thick HRH-10-1/8-4.0 Aramid fibre/phenolic resin Nomex. Facing skins were made of four plies of carbon epoxy AS4/8552 (0.000125 m) prepeg on both sides of the core with lay-up sequence of [90/45/45/90]. The test was done by dropping a suitable tup and mass arrangement from a defined height onto the required impact location of the test panels, in order to achieve the required impact energy. During the tests, the panel was placed on a cylindrical ring with an outer radius of 0.1016 m at the impact locations. The impactor tup diameters was 16 mm with a cylindrical mass attached to achieve the kinetic energy specified. Several low-velocity impacts with energy of 7–10 J were applied in four different positions. The tup was made of 1018 Steel. As in the case of CFRP plate, the scratched area around the impact source when exposed under UV radiation showed an evident contrast colour caused by the presence of the defect, thus providing remarkable results for the damage identification.

These results clearly show that the use of these nanoparticles Cu_2S to be included in paint or in a matrix would clearly make safety inspections of airplane exteriors easier. Impacts or other stresses would break the layers allowing a contrastingly coloured region, bringing attention to areas that may be weakened structurally.

This is especially important with modern aircraft made of fibre reinforced plastics which do not have the capability of metallic structures to absorb impact energy. By monitoring colour intensity changes or disruption with simple devices will alert inspectors to inspect damage that could otherwise prove easy to skip over.

5. Conclusions

The objective of this work was to develop a new smart polymer nanocomposite layer, with photoluminescence properties to be used for the detection of low-velocity impact damage on composite structures. It was shown a nanoscopic Cu_2S phase that can be generated by thermal decomposition of Cu(I) dodecylthiolate molecules dissolved into an amorphous polystyrene matrix. The thioether by-product acts as a strong capping-agent, which protect the nanoparticle and avoid their aggregation and growth. Owing to the very small size, a visible luminescence was observed for these polymer-embedded semiconductor nanoparticles. Luminescence can be excited by ultraviolet radiation of different wavelengths (300–400 nm), producing a strong and broad emission band extending from 600 nm to 800 nm. The broad emission band can be probably explained on the base of a contribution coming from the band-edge emission, and one coming from the trap-states. Moreover, this polymer nanocomposite incorporates electric and magnetic functionalities, thus it can be employed in different *in situ* Structural Health Monitoring (SHM) applications. A series of experiments based on low-velocity impact events at different energies were undertaken spreading the polymer nanocomposites layer on the surface of both carbon fibre and sandwich composite plates. The results indicated that the layer torn around the damaged area, produced a visible contrast colour whether irradiated by UV light, representing the flaw. This could be of particular benefit when rapid, cost-effective and not accessible visual inspection is required.

Further work is ongoing to refine and improve the fluorescence phenomenon, and to investigate the electro-magnetic properties of the smart nanocomposites layer for structural damage detection and to embed the nanoparticles in commercial paint or matrices.

References

[1] Balageas D, Fritzen CP, Güemes A. Structural health monitoring. ISTE Ltd; 2006.
[2] Alivisatos AP. J Phys Chem 1996;100:13226.
[3] Alivisatos AP. Science 1996;271:933.
[4] Carotenuto G, Martorana B, Perlo P, Nicolais L. J Mater Chem 2003;13:2927–30.

[5] Carotenuto G, Nicolais L, Perlo P. Polym Eng Sci 2006;46:1016.
[6] Carotenuto G, Longo A, Repetto P, Perlo P, Ambrosio L. Sensor Actuator B Chem 2007;125(1):202–6.
[7] Gubin SP, Kataeva NA, Khomutov GB. Russ Chem Bull 2005;54:827.
[8] Kreibig U, Vollmer M. Optical properties of metal clusters. Berlin: Springer-Verlag; 1995.
[9] Longo A, Pepe GP, Carotenuto G, Ruotolo A, De Nicola S, Belotelove VI, et al. Nanotechnology 2007;18:365701–6.
[10] Nicolais L, Carotenuto G. Metal-polymer nanocomposites. In: Carotenuto G, Nicolais L, editors. Hoboken, NJ: John Willey & Sons, Inc.; 2004.
[11] Nicolais F, Carotenuto G. Recent Patents Mater Sci 2008;1:1–11.
[12] Nicolais F, Longo A, Carotenuto G. Riv Italiana Compos Nanotecnol 2007;3(1):69–72.
[13] Sigman MB, Ghezelbash A, Hanrath T, Saunders AE, Lee F, Korgel BA. J Am Chem Soc 2003;125:16050.
[14] Turbeville W, Yap N. Catal Today 2006;116:519.
[15] Yang P, Song C, Lu M, Zhou G, Yang Z, Xu D, et al. J Phys Chem Solids 2002;63:639.
[16] Zhaoping L, Lang J, Xu D, Lu J, Qian Y. Chem Commun 2004;2724.
[17] Zhuge F, Li X, Gao X, Gan Z, Zhou F. Mater Lett 2009;63:652.